# NBS TECHNICAL NOTE 1065

U.S. DEPARTMENT OF COMMERCE / National Bureau of Standards

# Optical Time-Domain Reflectometer Performance and Calibration Studies

# NATIONAL BUREAU OF STANDARDS

The National Bureau of Standards[1] was established by an act of Congress on March 3, 1901. The Bureau's overall goal is to strengthen and advance the Nation's science and technology and facilitate their effective application for public benefit. To this end, the Bureau conducts research and provides: (1) a basis for the Nation's physical measurement system, (2) scientific and technological services for industry and government, (3) a technical basis for equity in trade, and (4) technical services to promote public safety. The Bureau's technical work is performed by the National Measurement Laboratory, the National Engineering Laboratory, and the Institute for Computer Sciences and Technology.

**THE NATIONAL MEASUREMENT LABORATORY** provides the national system of physical and chemical and materials measurement; coordinates the system with measurement systems of other nations and furnishes essential services leading to accurate and uniform physical and chemical measurement throughout the Nation's scientific community, industry, and commerce; conducts materials research leading to improved methods of measurement, standards, and data on the properties of materials needed by industry, commerce, educational institutions, and Government; provides advisory and research services to other Government agencies; develops, produces, and distributes Standard Reference Materials; and provides calibration services. The Laboratory consists of the following centers:

Absolute Physical Quantities[2] — Radiation Research — Chemical Physics — Analytical Chemistry — Materials Science

**THE NATIONAL ENGINEERING LABORATORY** provides technology and technical services to the public and private sectors to address national needs and to solve national problems; conducts research in engineering and applied science in support of these efforts; builds and maintains competence in the necessary disciplines required to carry out this research and technical service; develops engineering data and measurement capabilities; provides engineering measurement traceability services; develops test methods and proposes engineering standards and code changes; develops and proposes new engineering practices; and develops and improves mechanisms to transfer results of its research to the ultimate user. The Laboratory consists of the following centers:

Applied Mathematics — Electronics and Electrical Engineering[2] — Manufacturing Engineering — Building Technology — Fire Research — Chemical Engineering[2]

**THE INSTITUTE FOR COMPUTER SCIENCES AND TECHNOLOGY** conducts research and provides scientific and technical services to aid Federal agencies in the selection, acquisition, application, and use of computer technology to improve effectiveness and economy in Government operations in accordance with Public Law 89-306 (40 U.S.C. 759), relevant Executive Orders, and other directives; carries out this mission by managing the Federal Information Processing Standards Program, developing Federal ADP standards guidelines, and managing Federal participation in ADP voluntary standardization activities; provides scientific and technological advisory services and assistance to Federal agencies; and provides the technical foundation for computer-related policies of the Federal Government. The Institute consists of the following centers:

Programming Science and Technology — Computer Systems Engineering.

[1]Headquarters and Laboratories at Gaithersburg, MD, unless otherwise noted; mailing address Washington, DC 20234.
[2]Some divisions within the center are located at Boulder, CO 80303.

NBS technical note

# Optical Time-Domain Reflectometer Performance and Calibration Studies

B.L. Danielson

Electromagentic Technology Division
National Engineering Laboratory
National Bureau of Standards
Boulder, Colorado 80303

U.S. DEPARTMENT OF COMMERCE, Malcolm Baldrige, Secretary

NATIONAL BUREAU OF STANDARDS, Ernest Ambler, Director

Issued June 1983

National Bureau of Standards Technical Note 1065
Natl. Bur. Stand. (U.S.), Tech. Note 1065, 32 pages (June 1983)
CODEN: NBTNAE

U.S. GOVERNMENT PRINTING OFFICE
WASHINGTON: 1983

For sale by the Superintendent of Documents, U.S. Government Printing Office, Washington D.C. 20402
Price $3.50
(Add 25 percent for other than U.S. mailing)

CONTENTS

Table 1. List of Symbols, Nomenclature and Units

| Symbol | Nomenclature | Units |
|---|---|---|
| $A$ | Area | $m^2$ |
| APD | Avalanche photodiode | |
| $B$ | Noise bandwidth | Hz |
| $c$ | Velocity of light in vacuum | $ms^{-1}$ |
| $E$ | Electric field | $V/m^{-1}$ |
| EIA | Electronic Industries Association | |
| EMD | Equilibrium mode distribution | |
| $F$ | Noise figure | |
| $F_b$ | Backscatter constant | W |
| $G$ | Gain | |
| $h$ | Planck's constant | J/s |
| $I$ | Current | A |
| $I_b$ | Background radiation-induced current | A |
| $I_d$ | Bulk dark current | A |
| $i_c$ | Shot noise current | A |
| $i_n$ | Total noise current | A |
| $i_s$ | Signal current output from detector | A |
| $i_{th}$ | Thermal noise current | A |
| $k$ | Boltzmann constant | $J/K^{-1}$ |
| $K_B$ | Conversion gain | |
| $K_E$ | Electrical attenuation | |
| $K_o$ | Optical attenuation | |
| $L$ | Fiber length | m |
| $M$ | Multiplication gain factor | |
| $M^x$ | Excess noise factor | |
| NA | Numerical aperture | |
| NEP | Noise equivalent power | $W/Hz^{-1/2}$ |
| NDF | Neutral density filter | |
| ODR | Linear optical dynamic range | dB |
| OTDR | Optical time-domain reflectometer | |
| $P$ | Transmitted power | W |
| $P_b$ | Backscattered power | W |
| $P_{max}$ | Maximum optical power for linear responsivity | W |
| $P_{min}$ | Optical power for SNR = 1 | W |
| $q$ | Electronic charge | C |
| $R$ | Responsivity | $A/W^{-1}$ |
| $R_o$ | Responsivity at unit gain | $A/W^{-1}$ |
| $R_d$ | Reverse junction resistance | $V/A^{-1}$ |
| $R_s$ | Series contact resistance | $V/A^{-1}$ |
| $R_{sc}$ | Effective space charge resistance | $V/A^{-1}$ |
| SNR | Signal-to-noise ratio | |
| $t$ | Time | s |
| $V$ | Voltage | V |
| $V_d$ | Detector output voltage | V |
| $V_o$ | Recorder output voltage | V |
| $v$ | Group velocity | $ms^{-1}$ |
| $v_d$ | Drift velocity | $ms^{-1}$ |
| $W$ | Width of avalanche region | m |
| $Z_L$ | Load impedance | $V/A^{-1}$ |
| $\alpha$ | Attenuation per unit length | $db/km^{-1}$ |
| $\beta$ | Loss coefficient | $m^{-1}$ |
| $\varepsilon$ | Dielectric constant | $F/m^{-1}$ |
| $\eta$ | Quantum efficiency | |

# Optical Time-Domain Reflectometer Performance and Calibration Studies


B. L. Danielson*

National Bureau of Standards
Boulder, Colorado 80303



The measurement accuracy of the optical time-domain reflectometer (OTDR) is restricted in some applications by a limited operational dynamic range and by a lack of standardized test procedures. In an effort to better understand these restrictions, we have measured the range of linearity of some avalanche photodiodes used as backscatter detectors. Also, the effect of input launch conditions is examined and a possible standardized OTDR test procedure is proposed. Using these suggestions, we have made comparisons between attenuation values determined by cutback and backscatter methods and found that good agreement is possible. Finally, some methods are described for checking the response linearity of OTDR systems.



Key words: APD; avalanche photodiodes; backscattering; backscatter signatures; optical fiber scattering; optical time-domain reflectometer; OTDR.


## 1. Introduction

The optical time-domain reflectometer is a versatile instrument that finds many applications in optical fiber diagnostics and in the estimation of various waveguide parameters [1]. In this device, optical power is launched into the fiber or cable in the form of a short (5 to 100 ns) pulse and the Rayleigh backscattered light, as well as reflections from imperfections and joints, is recorded as a function of time. The analysis of this signature can yield much useful information regarding the nature and location of faults and external perturbations. In addition, the OTDR can give quantitative estimates of attenuation, impulse response, fiber diameter fluctuations, fiber or cable length, and splice or connector loss. Backscatter methods are not without their limitations, however. The accuracy of parameter estimates which can be obtained with this approach often suffers in comparison with other measurement techniques. The present work is part of a continuing study of the applicability of this backscatter method for accurate fiber characterization. Previous reports in this series were concerned with the effect of fiber inhomogeneities on attenuation values [2], the description of experimental methods [3], and the analysis of signatures under a variety of experimental conditions [4]. Here we will consider two issues which bear on the reproducibility and ultimate accuracy of OTDR measurements: linearity of response of the avalanche photodiode detectors (APDs), and the effect of


*Electromagnetic Technology Division, Center for Electronics and Electrical Engineering.

launch conditions on attenuation in graded-index fibers. These two problems are treated separately in sections 3 and 4, respectively. The problem of linearity is crucial since backscatter systems routinely operate over a very large range of incident optical power. Also standardized operating conditions for the launch and recovery of radiation are necessary for consistency and for good agreement between backscatter and other methods for determining fiber attenuation. Some possible preferred procedures for OTDR systems will be discussed.

## 2. Review of APD Operation

The main concern of this section is the review of some of the properties of backscatter radiation detectors which affect the performance of OTDR systems. Although photomultiplier tubes have been used occasionally in this type of application, the avalanche photodiode detector is preferred due to its small dimensions, insensitivity to overload, fast response, and modest bias voltage requirements. The scope of the treatment here will be restricted to the wavelength interval from 800 to 900 nm where most backscatter systems operate. In this region, silicon APD detectors are used almost exclusively since they have high quantum efficiency and low noise properties relative to other semiconductor materials. These devices are important in optical communication systems, and as a consequence have been the object of an intense development effort. Their characteristics have been well documented in a number of recent review articles which we will draw on in the following discussion [5-20].

### 2.1 Sensitivity Considerations

Most optical time-domain reflectometers routinely operate with received optical power in the range of nanowatts. At such small power levels, and with broadband detection, it is difficult to process the signals electronically without adding excessive noise. For this reason, most backscatter systems use APD detectors which are capable of low-noise avalanche gain in the detector itself. The gain mechanism in this case is based on collisional ionization as shown in figure 2-1. In the case of silicon detectors, electrons have higher ionization coefficients than holes, and are responsible for the bulk of the gain. These carriers are accelerated in the high electric field region to energies sufficient to produce secondary carriers in a collisional process. The secondaries themselves undergo ionizing collisions. Overall gains are typically about 100 or so. Some excess noise is introduced by the multiplication process but the overall sensitivity nevertheless is improved significantly over detectors which do not possess internal gain.

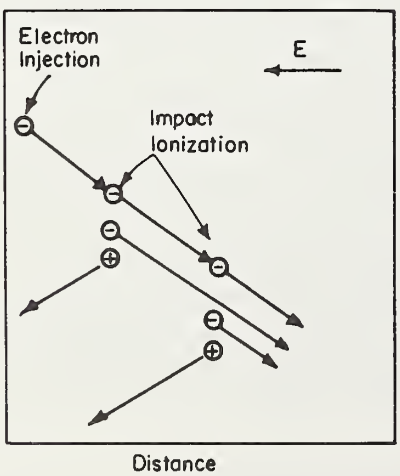


Figure 2-1. Schematic representation of the avalanche multiplication process in the high-field region of a back biased silicon p-n junction. Pair generation is predominantly by electrons. The direction of the electric field E is indicated by the arrow (after Melchoir [19]).

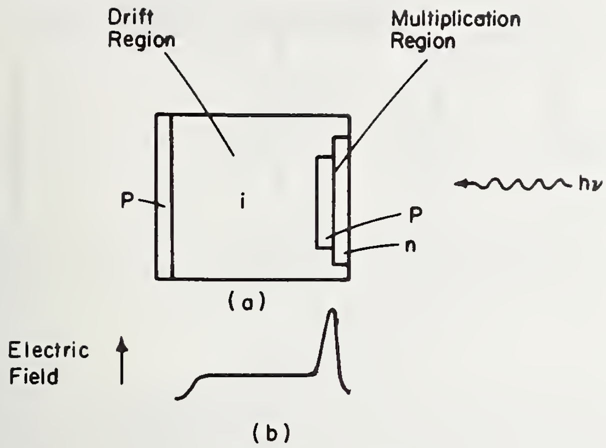


Figure 2-2. (a) Typical structure of a reach-through type silicon avalanche photodiode. Radiation enters the detector from the right.
(b) The electric field in the detector. The horizontal scale is the same as in a.

## 2.2 Principles of Construction and Operation

Many diverse solid-state avalanche photodiode types and structures have been reported in the literature [14]. Specific properties, for example fast response, high gain, or low noise, can often be tailored by specific device construction. We will restrict our discussion here to a particular subclass of APDs which are usually referred to as the "reach-through" type. These detectors have several desirable characteristics and are probably the most common in optical communication systems. The experimental work in this report (section 3) was confined to this sort of detector. At the present time they are available commercially from a number of vendors [21].

A schematic representation of the diode configuration of a reach-through avalanche photodiode is shown in figure 2-2a. The corresponding electric field profile is given in figure 2-2b. When such a detector is back biased, an electric field is created in the neighborhood of the p-n junction due to the removal of mobile carriers. This region is called the depletion layer. As the applied electric field is increased, the depletion layer of the diode "reaches through" to the almost intrinsic i region. The bulk of the incoming radiation is absorbed in the i region, and the resulting photogenerated electrons drift to the high-field zone where avalanche multiplication occurs. The light is shown in figure 2-2a entering the device from the right; operation is also possible for radiation entering through the other face. This type of structure has several distinct advantages. In addition to a fairly fast response time and high gain characteristic, the regions of photon absorption and carrier multiplication are separated. This insures uniform multiplication statistics, resulting in low noise [13]. Generation of electron-hole pairs within the multiplication region is also undesirable since it reduces the effective multiplication factor. In addition, the reac-through geometry results in an negligible "diffusion tail" on the impulse response [22]. In some detectors carriers can be generated in low-field regions. Since the carriers must undergo a relatively slow diffusion to the high-field region, the impulse response has a long fall time--often many microseconds in duration. Diffusion tails obviously are undesirable for OTDR applications where the slow component due to the initial Fresnel reflection from the input end could obscure the signal backscattered from remote parts of the fiber.

A typical circuit application is shown in figure 2-3a. The detector is backbiased at a voltage of a few tens to a few hundreds of volts, depending on device structure. A large capacitor C provides a constant voltage to the APD during high peak pulse operation and allows for a low impedance ac return. The resistor $R_L$ is a physical load resistor.

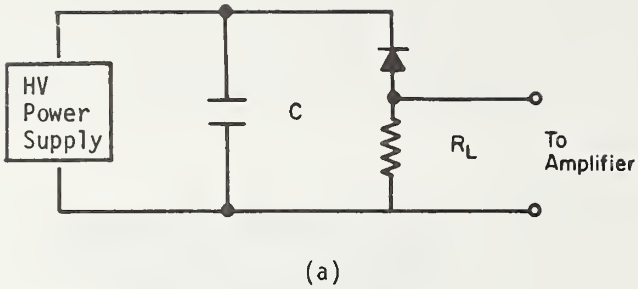


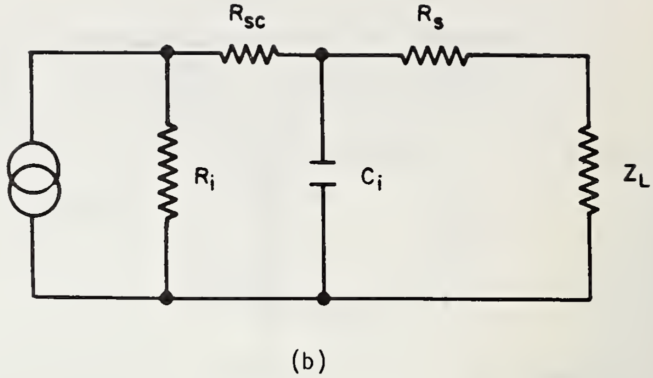


Figure 2-3. (a) APD biasing circuit. $R_L$ is the load resistance, and C a large capacitance. (b) APD simplified equivalent circuit. The detector can be approximated by a current source. $R_s$ is the diode contact resistance, $R_{sc}$ the effective space charge resistance, $R_i$ and $C_i$ the internal impedance. Here, $Z_L$ is the effective load impedance which includes the load resistance and the input impedance of the preamplifier (adapted from ref. 7).

A simplified equivalent circuit appropriate for OTDR applications is illustrated in figure 2-3b. This circuit may be described in terms of the following parameters [7]:

$C_i$ Diode capacitance

$I_d$ Bulk dark current component which undergoes multiplication. This originates from spontaneous effects in the depleted layer and photodetector surface.

R Detector responsivity

$R_d$ Reverse junction resistance

$R_s$ Series contact resistance

$R_{sc}$ Effective space charge resistance

$Z_L$ Load impedance including preamplifier input resistance

The current source is equal to $(P_oR + I_d)$ M, where $P_o$ is the optical power impinging on the detector. The bulk dark current $I_d$ is typically $3 \times 10^{-11}$ to $1.0 \times 10^{-10}$ A/mm$^2$. In addition, there is a surface dark current component which is not multiplied whose magnitude is around 50 nA. We have neglected this latter component since usually it is not the dominant contribution to the noise current in small area detectors at high gains. We have also assumed the background induced current to be zero in this case. The reverse junction resistance $R_d$ is usually large enough ($10^{10}$ Ω) to be ignored. The diode series contact resistance $R_s$ is typically a few ohms. The effective space charge resistance $R_{sc}$ is not a physical resistance (it does not affect the rise time of the device) but is useful in describing saturation effects to be described in section 2.4. A typical value is about 2000 Ω. The junction capacitance $C_i$, of a few picofarads, must be kept low to insure a good speed of response.[1]

[1]For most reach-through APDs operated at gains near one hundred, the response time is determined by drift transit time in the i region. In some wide bandwidth structures the time required for the multiplication process will dominate the response speed. In this case, the APD can be characterized by a constant gain bandwidth product; the higher the gain, the slower the response. Usually the multiplication time will dominate if the gain-bandwidth product is greater than about a hundred gigahertz.

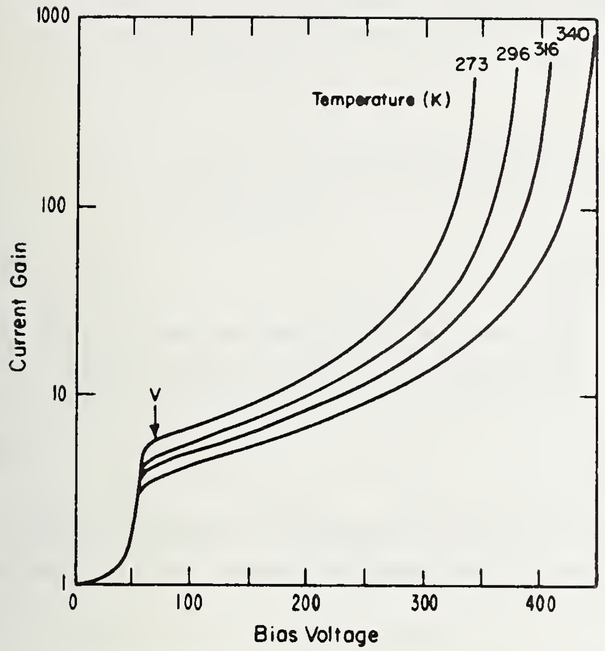


Figure 2-4. Current-gain versus voltage characteristic for a silicon APD at different temperatures, measured at 825 nm (adapted from Melchoir [23]). In order to avoid "diffusion tails" on the impulse response, the APD should be biased above the voltage V which fully depletes the i region.

## 2.3 Temperature Effects

An important property of APDs, especially in field applications, is their temperature dependence. Although at wavelengths of 950 nm or less the quantum efficiency is approximately independent of temperature,[2] the avalanche gain is a strong function of temperature (as well as bias voltage); increasing the temperature decreases the gain. Figure 2-4 shows the gain-bias voltage curves for several temperatures for a typical reach-through photodiode. In this diagram, the voltage V indicates the threshold at which the absorption region becomes fully depleted, usually when multiplication values reach 2 to 20. Normal bias voltages lie above this value. One quoted figure for an APD temeprature-gain dependence is given in reference 23. Here, 1.4 V of bias voltage increase is required for each degree Celsius change in temperature in order to keep the gain constant. This figure will vary according to the width of the depletion region. Since the gain is a temperature-dependent parameter, the detector often must be stabilized by feedback control in order to insure accurate signature acquisition.

## 2.4 Saturation Effects

The operational power limits of the APD detector largely determine the dynamic range of the OTDR, which is a critical performance specification in backscatter applications. At high optical power levels the detector undergoes nonlinear effects, particularly gain saturation. The principal mechanisms responsible for these nonlinearities are:

A. Large currents across the series resistance or load resistance decrease the effective bias voltage.

B. Space charge effects may decrease the electric field in the gain region. The reduction in field leads to a current-dependent reduction of the carrier multiplication factor. This can be seen as follows. The current flowing in the avalanche region reduces the electric field by an amount given by the relation [24]

[2] At 1060 nm the quantum efficiency increases rather dramatically with temperature.

$$\Delta E = \frac{IW}{2\varepsilon v_d A} \tag{2-1}$$

with

$I$ current in avalanche region of diode

$W$ width of avalanche region

$\varepsilon$ dielectric constant of silicon

$v_d$ average drift velocity of carriers

$A$ illuminated device area.

The field is associated with an effective bias voltage change of $W\Delta E$. Then the space charge effect can be identified with a resistance $R_{sc}$ in the equivalent circuit of figure 3-1b as

$$R_{sc} = \frac{W^2}{2\varepsilon v_d A}. \tag{2-2}$$

The effect of this resistance is to create a current-dependent reduction in the carrier multiplication factor. Equation (2-2) implies that radiation focused to smaller spot sizes will saturate the detector at lower optical power levels.

C. High optical power levels may cause local heating. The resulting increase in temperature decreases the gain.

Also, gain nonuniformities over the surface of the detector and microscopic defects complicate these processes. In general, the saturation behavior will be a function of material parameters, the device structure, and the incident radiation wavelength [14]. In addition to the detector effects, the preamplifier associated with the APD may exhibit a nonlinear response at high peak current levels. For optical power levels less than the saturation level, the APDs typically show excellent linearity [7].

## 2.5 Signal-to-Noise Ratio and Dynamic Range Considerations

As we have seen, the maximum optical power compatible with linear operation of the OTDR, $P_{max}$, is determined by saturation effects. For very weak optical signals, on the other hand, the sensitivity will be impared by the masking effects of noise. We will now examine some of the more important sources of noise in detectors, and derive an expression for the effective dynamic range of the detector for a given signal-to-noise ratio (SNR).

The noise in APD detectors is of two basic types:

A. Current shot noise with a mean square value given by

$$\overline{i_c^2} = 2\,q\,(I_s + I_b + I_d)\,M^{2+x}\,B \tag{2-3}$$

with

$q$ electronic charge ($1.602 \times 10^{-19}$ C)

$I_s$ photogenerated primary signal current

$I_b$ background radiation induced signal

$B$ noise bandwidth

$M$ multiplication factor

$M^x$ excess noise factor (x approximately 0.3 to 0.5)

and other terms defined as before.

This shot noise is due to current fluctuations arising from the discrete nature of the photogenerated carriers in the detector, and the fact that the generation of the electron-hole pairs is not completely deterministic. This type of noise will generally dominate in optical receivers when signal current levels are large.[3]

B. Thermal noise of the detector-preamplifier considered as a unit, with a mean square value which can be approximated as

$$\overline{i_{th}^2} = \frac{4\ k\ T\ F\ B}{Z_L} \tag{2-4}$$

with

k Boltzmann constant ($1.380 \times 10^{-23}$ J/K)

T temperature K

F preamplifier noise figure. In some cases this may be bandwidth dependent. In general, it is a function of load impedance.

$Z_L$ effective detector load impedance, including input impedance of preamplifier.

This source of noise is also termed Johnson noise. For Gaussian noise processes the total noise current variance $\overline{i_n^2}$ is just the sum of $\overline{i_c^2}$ and $\overline{i_{th}^2}$ or

$$\overline{i_n^2} = \overline{i_c^2} + \overline{i_{th}^2} = 2q(I_s + I_b + I_d)M^{2+x}\ B + 4\ k\ T\ F\ B/Z_L. \tag{2-5}$$

For direct detection, the output (electrical) signal-to-noise ratio is now defined to be

$$\text{SNR} = \left(\frac{i_s}{i_n}\right)^2 = \frac{i_s^2}{2q(I_s + I_b + I_d)M^{2+x}B + 4k\ T\ B\ F/Z_L}. \tag{2-6}$$

where $i_s$ is the signal current amplitude after amplification, and is related to the incident optical power $P_o$ by the relation

$$i_s = R\ P_o = R_o\ M\ P_o. \tag{2-7}$$

Here R is the detector responsivity (A/W) with the corresponding unity gain responsivity $R_o$. This latter quantity may also be expressed as

$$R_o = \frac{q\eta\lambda}{h\ c} \tag{2-8}$$

with the usual notation:

$\eta$ quantum efficiency,

$\lambda$ wavelength of light,

h Planck's constant, and

c velocity of light in vacuum.

[3]The signal-dependent component of this noise, eq (2-6) with $x = I_b = I_d = 0$, is referred to as the quantum noise. In an ideal receiver quantum noise will dominate over thermal noise if $h\nu \gg kT$.

If the wavelength is expressed in micrometers, this becomes, approximately

$$R_o \approx 0.806\ \lambda\eta. \tag{2-9}$$

Equation (2-7) makes explicit the fact that APDs are square-law detectors; that is, electrical power output by the detector is proportional to the square of the optical power.

Melchior [19] has shown that the SNR in eq (2-6) is maximized when the avalanche gain is increased to the point where the shot-noise term is just equal to the thermal-noise term. In this case, the minimum detectable signal is lower by a factor of approximately $\sqrt{2}/M$ over a comparable thermal noise limited detector with M = 1. In actual operating systems, however, the maximum achievable gain is often set by device constraints of saturation effects. Also, eq (2-6) shows that, other quantities remaining constant, as the load impedance $Z_L$ increases the SNR is improved. This can be accomplished by using a transimpedance amplifier in close proximity with the detector.

A convenient quantity for expressing noise performance at the lower limit of detector sensitivity is the minimum detectable optical power, $P_{min}$. This is defined to be the optical power incident on the APD which gives rise to a signal current just equal to the total noise current from the detector. Under these conditions, the SNR in eq (2-6) is equal to unity and we can write

$$P_{min} = \frac{hcB}{\eta\lambda}\left(M^x + \left\{M^{2x} + \frac{1}{Bq}\left[(I_b + I_d)M^x + \frac{4\ k\ T\ F}{M^2\ q\ Z_L}\right]\right\}^{1/2}\right). \tag{2-10}$$

Another parameter often used to indicate noise performance is the noise equivalent power (NEP), usually defined to be the minimum detectable power normalized to unit bandwith,[4] or

$$NEP = \frac{P_{min}}{\sqrt{B}}. \tag{2-11}$$

The linear optical dynamic range (ODR) of the detector in decibels can then be written as

$$ODR = 10\ \log\left(\frac{P_{max}}{P_{min}}\right) = 10\ \log\left(\frac{P_{max}}{NEP\sqrt{B}}\right). \tag{2-12}$$

In the next section we will determine the values of $P_{max}$ and ODR for several APD detectors which have been used in OTDR systems.

## 3. Linearity Measurements

### 3.1 Measurement Methods

In this section we describe measurements on the responsivity of several reach-through avalanche photodiodes. At high levels of incident radiation, all the detectors are observed to undergo saturation in the responsivity. From these measurements the maximum power for linear operation can be determined. The experiment was designed to test the APDs under conditions closely approximating those encountered in the time-domain reflectometer which has been described in detail elsewhere [3].

[4] In some cases, detector NEP is given without specifying the associated amplifier properties or load resistance. In our context, this type of NEP figure would only be meaningful if the dark current term is the predominant source of noise in eq (2-10). This is possible with state of the art amplifiers and small-area detectors with gains greater than about 30 [7]. In this case, $P_{min} = \sqrt{(qI_dM^xB)}/R_o$. This is not a very sensitive function of the multiplication gain. Using a bandwidth of 100 MHz, this minimum power can be a few tenths of a nanowatt. Also, we can see from eq (2-10) the NEP is independent of bandwidth only under these limiting conditions.

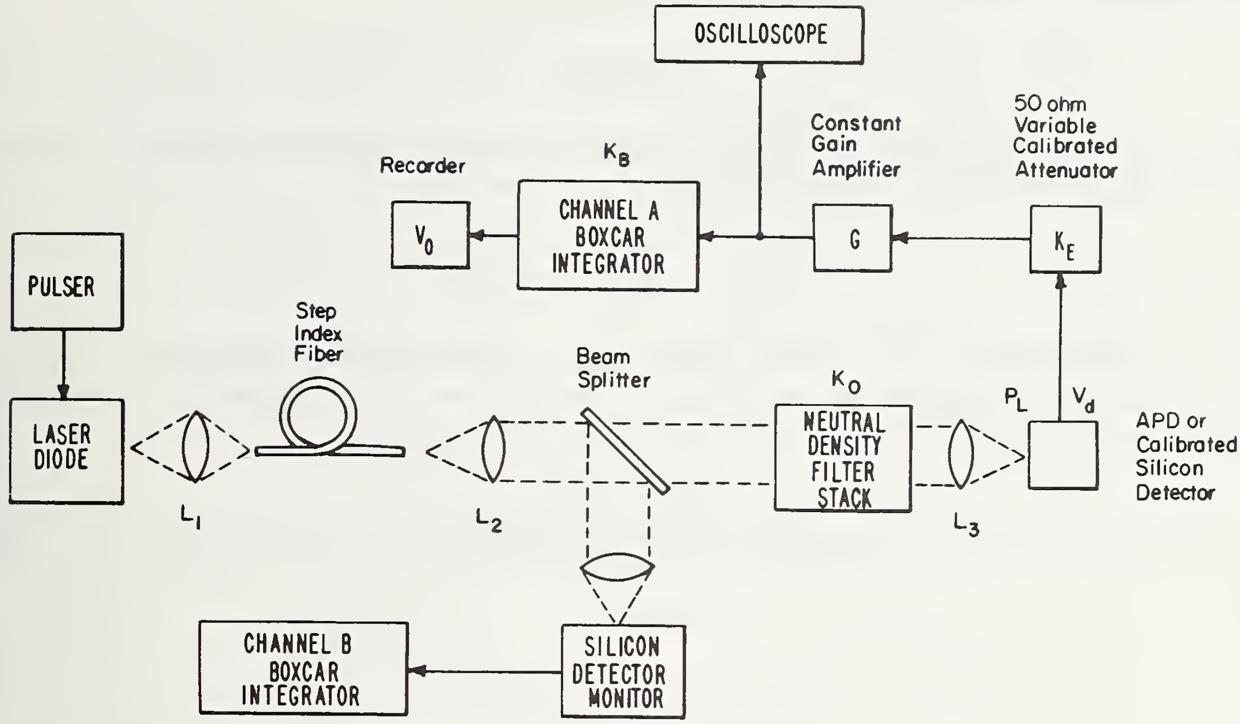


Figure 3-1. Apparatus for measuring APD response linearity.

The measurement apparatus is illustrated in figure 3-1. A single heterojunction GaAlAs laser diode operating at 850 nm is used as a source. The output optical pulse has a full width half maximum of about 18 ns. Since the laser emission has a stripe geometry, a more uniform source distribution can be obtained by injecting the radiation into a short length of step-index fiber which acts as a mode scrambler. The fiber output emitting surface is then a fairly uniform spot of about 50 μm diameter. The microscope objective lens $L_2$ collimates this radiation which is then attenuated by calibrated neutral density filters (NDFs) and focused on the test detector mounted on a micropositioner. A calibrated silicon PIN detector (EGG model SGD 100A) [25] may be inserted in the same position to measure the power level at that point, and also to calibrate the NDFs.[5] The test spot size is given by the launch spot size multiplied by the ratio of focal lengths of lenses $L_3$ and $L_2$. The detection system consisted of a two-channel boxcar integrator with an X-Y recorder readout (as in the OTDR), a constant gain G = 100 amplifier, and a variable calibrated electrical attenuator (50 Ω, HP models 355D and 355E). The electrical attenuation $K_E$ was adjusted so as to produce a nearly constant input to the signal processor. The boxcar integrator was tuned to measure the peak pulse amplitude with a conversion gain of $K_b$. A silicon detector-beamsplitter arrangement was used to insure a constant amplitude optical pulse input to the optical attenuators. The second channel of the boxcar averager was used to process this monitor signal. Under these conditions the voltage at the output of the detector $V_d$ is related to the recorder output voltage $V_o$ by the relation

$$V_d = \frac{V_o}{F_B K_E G}. \tag{3-1}$$

[5]Silicon detectors can also exhibit saturation effects. In the detector used here, observable changes in responsivity occur at optical powers as small as 1 mW with a spot size of 39 μm.

The power actually impinging on the detector $P_L$ is

$$P_L = K_0 P_{L0} \tag{3-2}$$

where $P_{L0}$ is the measured optical power with no optical attenuation $K_0$ in the input beam. The responsivity of the detector with a 50 Ω load resistance $Z_L$ is then given by

$$R = \frac{V_d}{P_L Z_L}. \tag{3-3}$$

Since we are interested here only in the relative outputs, somewhat greater measurement accuracy can be obtained if we normalize the responsivity by taking the ratio of the responsivities at high- and low-power levels. Then

$$\frac{R}{R(1)} = \left(\frac{P_L(1)}{P_L}\right)\left(\frac{K_E(1)}{K_E}\right)\left(\frac{V_o}{V_o(1)}\right) \tag{3-4}$$

where

$$P_L(1) = K_o(1) P_{Lo} \tag{3-5}$$

and the subscript 1 refers to the average value of the quantity in question at low optical power levels. Then using eqs (3-2), (3-4), and (3-5) we can determine the relative responsivity as a function of absolute optical power level.

## 3.2 Results

Three commercial reach-through APDs were examined for saturation effects under differing conditions of bias voltage and spot size. For reference purposes, the manufacturer's nominal specifications are listed in table 2. Detectors A and B were discrete types, while detector C was a modular type with an integral preamplifier.

The normalized responsivity for the three test detectors is shown in figures 3-2 to 3-4. If we arbitrarily define $P_{max}$ as that peak optical power at which the relative responsivity drops to 0.8, we can see that the values lie in the range $5 \times 10^{-7}$ to $2 \times 10^{-5}$ W.[6] The response of detector C is determined in part by the associated preamplifier rather than the photodiode itself. The saturation value decreases with spot size as would be expected from eq (2-2). A lower bias voltage increases the saturation value. There is also some indication that small nonlinearities may occur in the gain at power levels below the onset of saturation. The individual results for the detectors under the various test conditions are summarized in table 3. We have taken the optical dynamic range equal to be $10 \log(P_{max}/NEP \cdot B^{0.5})$ from eqs (2-11) and (2-12). We have also assumed a bandwidth of 100 MHz and used the manufacturer's quoted NEPs in these calculations.

[6] A $P_{max}$ of about $6 \times 10^{-5}$ W has been reported by Melchoir [26] at 488 nm in a silicon avalanche photodiode.

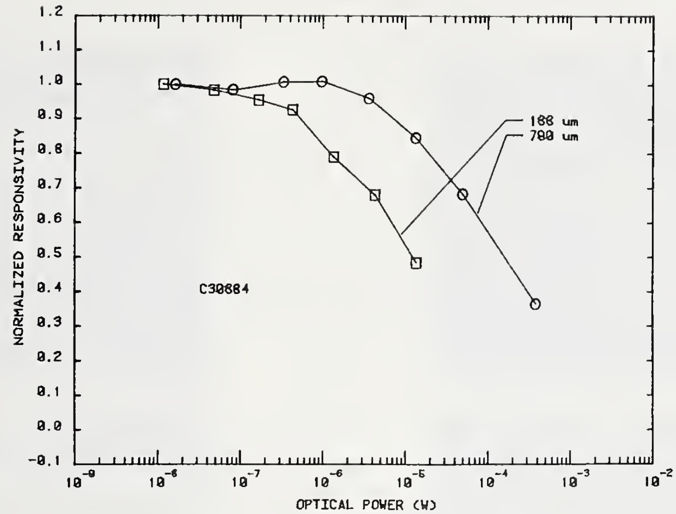


Figure 3-2. The normalized responsivity for detector A. The radiation is focused on the detector with spot diameters of 188 and 790 μm. Operating voltage is 280 V in both cases.

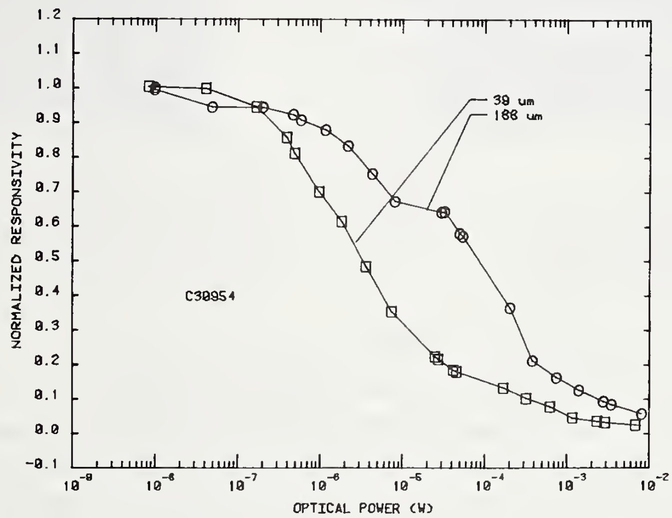


Figure 3-3. The normalized responsivity for detector B. The radiation is focused on the detector with spot diameters of 39 and 188 μm. Operating voltage is 423 V in both cases.

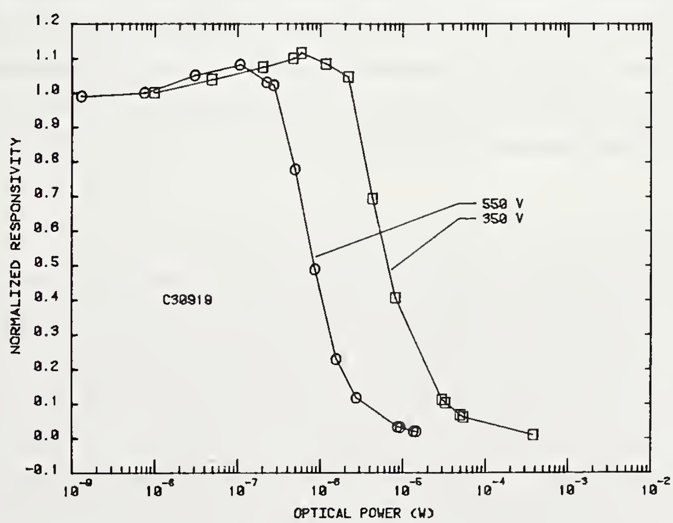


Figure 3-4. The normalized responsivity for detector C. The two bias voltages are indicated. The spot size in both cases is 188 μm.

Table 2. Nominal specifications of the APDs tested in this work

| Detector | Photosensitive surface diam. mm | Maximum bias voltage V | Avalanche breakdown voltage V | NEP $W/Hz^{-1/2}$ | R @ 900 nm A/W |
|---|---|---|---|---|---|
| A | 0.8 | 285 | 311 | $1.3 \times 10^{-14}$ | 61 |
| B | 0.8 | 423 | 473 | $1.2 \times 10^{-14}$ | 36[a] |
| C[b] | 0.8 | 550 | --- | $2 \times 10^{-14}$ | $2 \times 10^{4}$ |

[a] At 1060 nm
[b] Detector/preamplifier module

Table 3. Maximum power and dynamic range for linear operation of test photodiodes

| Detector | Spot size µm | Bias voltage V | $P_{max}$ W | Dynamic range[a] dB |
|---|---|---|---|---|
| A | 188 | 280 | $1.3 \times 10^{-6}$ | 40 |
| A | 790 | 280 | $2.0 \times 10^{-5}$ | 52 |
| B | 39 | 423 | $5.1 \times 10^{-7}$ | 36 |
| B | 188 | 423 | $3.0 \times 10^{-6}$ | 44 |
| C | 188 | 550 | $4.9 \times 10^{-7}$ | 34 |
| C | 188 | 550 | $3.4 \times 10^{-6}$ | 42 |

[a] Assumed bandwidth: 100 MHz

Some representative APD output pulse shapes are shown in figures 3-5 and 3-6. The response in (a) in both figures is from a relatively low power optical input pulse. The corresponding response in (b) is from an optical pulse whose power level is considerably above the saturation threshold for the detector. The electrical pulses have been attenuated so that the oscilloscope displays are on the same scale. It can be seen that, except for some barely perceptible ringing at the high-power levels, the two responses of detector B (fig. 3-5) are very similar. The behavior of detector A (not shown) is nearly identical. This demonstrates that the photodiode itself recovers from overload on a time-scale much shorter than the pulse duration used in this experiment. On the other hand, the response of detector C (fig. 3-6) has a recovery time that increases with optical power at and above $P_{max}$. It will be recalled (table 2) that this detector has a built-in preamplifier. Apparently, the amplifier is responsible for the observed recovery effects.

### 3.3 Discussion of Results

It is clear from the experimental data that there is a wide variability in the responses of the APDs. These differences are related to the detector type, operating conditions, and associated preamplifier. For maximum linear dynamic range the entire photosensitive surface should be illuminated. With detectors having integral light pipes this is not a problem, but some care is required when beam optics are used. Also, the dynamic range can be improved somewhat in certain cases by the simple expedient of reducing the bias voltage. As long as the internal gain is sufficient for the shot noise to dominate over amplifier thermal noise, there is little advantage to further increasing M. Finally, the preamplifier must be carefully designed so that it does not cause excessive distortion at high peak powers.

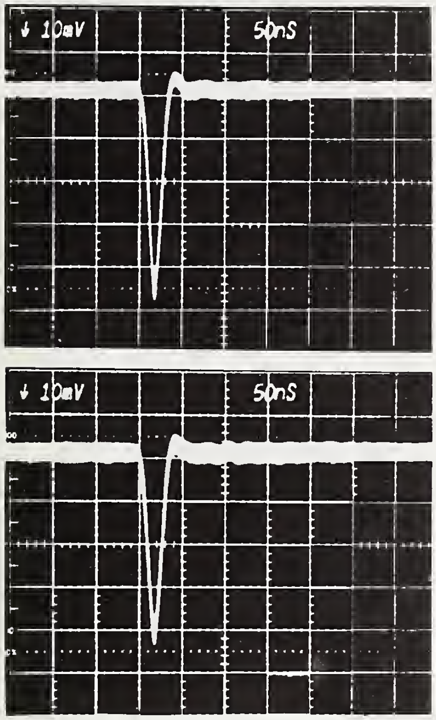


Figure 3-5. Response of detector B as a function of time for different input power levels: (a) $1.6 \times 10^{-7}$ W, (b) $7 \times 10^{-3}$ W.

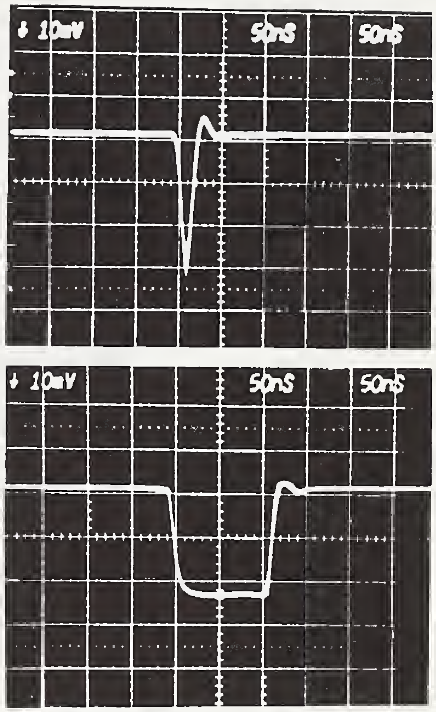


Figure 3-6. Response of detector C as a function of time for different input power levels: (a) $5 \times 10^{-8}$ W, (b) $3 \times 10^{-5}$ W.

### 3.4 Linearity Checks

Since there is such a wide range of possible photodiode response patterns, it is desirable to have simple linearity checks which can be applied to actual OTDR systems under operating conditions. We mention three possibilities here.

1. A reference test fiber can be used. The attenuation as a function of length (which implies the optical power to the detector is a function of time) can be compared with measurements made on the same fiber by other observers. Under specific and controlled experimental conditions, the OTDR response can be precisely characterized in this manner. Such a test sample (fiber c), to be described in section 4, is available at NBS. It is one of the fibers which has undergone attenuation measurements by the two-point or cutback technique in a series of interlaboratory comparisons.
2. A simple qualitative check for saturation effects involves comparison of the optical attenuation values of any test fiber made under normal operating conditions with those made under reduced bias voltage or laser diode power; lower values of apparent fiber attenuation under reduced conditions indicate the possibility of saturation effects.
3. A more quantitative check can be made if beam optics are used in the OTDR system. In this case, a reference absorption-type neutral density filter is inserted in the backscatter beam at some point where the signal beam is approximately collimated (see fig. 3-7). The filter should have a small attenuation value (e.g., an optical density of 0.1) but need not be calibrated. The fractional change in the initial (t = 0) backscatter amplitude is noted. This filter is then removed and another arbitrary neutral density filter inserted in the beam to

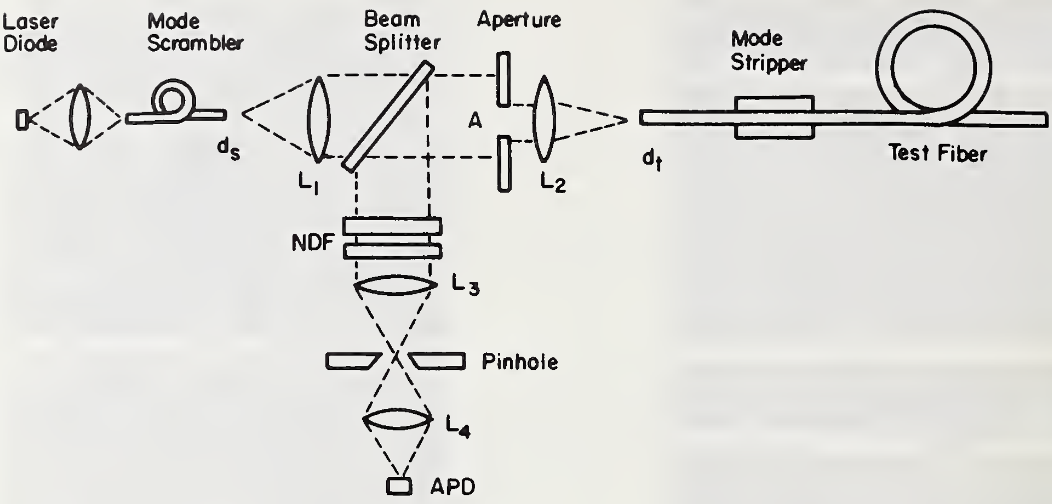


Figure 3-7. Schematic of an OTDR system illustrating the position of neutral density filters for checking the APD response linearity. Lenses $L_1$, $L_2$, $L_3$, and $L_4$ are focusing and collimating microscope objectives. The function of the pinhole and aperture are explained in section 4.3.

change the power level at the detector. The reference filter is again put in the beam and the fractional change in backscatter amplitude noted as before. This procedure is repeated for many different power levels. If the system is linear, the same fractional change in backscatter power is observed at each measurment point. However, it is not convenient to implement this method if, as is often the case, directional couplers and pigtailed light-pipe type detectors are used in the OTDR.

## 4. OTDR Attenuation Measurements

Optical fiber attenuation is one of the more important parameters which can be estimated from an analysis of the backscatter signature. It can be shown [27] that, for fibers that have uniform transmission properties as a function of length and whose properties are the same in both directions, the backscattered power $P_b(t)$ is of the simple exponential form

$$P_b(t) = F_b e^{-\beta vt} \tag{4-1}$$

where $F_b$ is the backscatter constant and v the known group velocity of propagation of radiation and t the time. In this case, the slope on a semilogarithmic plot of power versus time yields a convenient value for the fiber loss $\beta$ (nepers/m). Fiber attenuation rates are usually expressed in units of $\alpha$ (dB/km), where $\alpha \simeq 4.343 \times 10^3\ \beta$. Unfortunately, many fibers encountered in practice do not obey exactly this simple exponential relationship. There are many possible reasons for this [3]. Most of these reasons have to do with the fact that some fibers (usually poor quality fibers) are not good approximations to the homogeneous transmission medium we have assumed in the derivation of eq (4-1). Under these circumstances it may not be a straightforward matter to extract accurate attenuation values from the backscatter signature, at least from single-ended measurements. Divita and Rossi have shown [28] that it is possible to separate the fiber loss from other parameter fluctuations if backscatter measurements can be made from both fiber ends. In some cases, improved OTDR loss values can be made by simply averaging the attenuation (in dB) obtained from measurements made in this way.

There are three principal techniques for measuring attenuation in optical fibers. These are referred to as the cutback, insertion, and backscatter methods. It is now generally agreed that the cutback and insertion methods (to be described in detail in section 4.2) are the more accurate when compared with the backscatter approach. They offer better signal-to-noise ratios, and entail better control of launch conditions. Also, they are not prone to signal misinterpretation when fiber irregularities are encountered. Although OTDR loss determinations are generally not considered in standard test procedures, they are often used in applications where the more accurate methods are not convenient (due to their complexity) or not possible (for example, when only one end of the fiber or cable is accessible). It is desirable then to explore experimental backscatter techniques which lend themselves to good agreement with accepted reference attenuation test procedures. With this end in mind, we will review the generally-accepted test procedures for attenuation, and discuss experimental OTDR configurations which provide launch conditions compatible with these standard methods. In particular, we will investigate the effect of a mandrel wrap mode filter on the backscatter-derived attenuation values. These devices are also used in controlling the launch mode volume in some types of cutback attenuation systems.

In the present work, we will be concerned only with fiber attenuation values though the recommended backscatter test conditions have application to splice loss estimates as well.

## 4.1 Significance of Launch Conditions

It is a well-known fact that test launch conditions can have a significant effect on measured attenuation values in multimode fibers. In some early work [29], a spread of up to 2 dB/km was noted in attenuation values which were attributed to differences in the way light was launched into the test fiber. The reason for this dependence has its origin in the fact that, in many multimode fibers, each propagating mode group exhibits its own characteristic loss rate. Generally (but not always), higher-order guided modes will have loss values greater than the mean [30]. The increased losses for higher-order modes can arise from such factors as microbending, leaky modes, core-cladding interface scattering, and the effect of lossier cladding material.[7] This situation implies that, if the fiber initially has all the modes excited by the input radiation, the attenuation will be a function of length as the higher-loss modes are extinguished closer to the launch end. For fibers with appreciable amounts of mode mixing, the power lost to the lossy modes at some point in the fiber will be exactly replenished by power coupled in from other modes. This leads to the creation of an equilibrium mode distribution (EMD). Once this energy balance prevails the modal power distribution no longer changes with length, and the far-field pattern is independent of the input launch conditions.[8] Measurement of attenuation under EMD conditions is obviously desirable for specifications and system design purposes. One difficulty with this whole concept is the fact that many modern fibers have very little mode

[7]Loss may also increase for the lowest-order modes due to excess Rayleigh scattering from dopant concentration fluctuations in the center of the parabolic-index fiber.

[8]The "steady-state" modal distribution is a similar abstraction, defined as a situation in which the far-field radiation patterns are the same in both short and long lengths of fiber. As an example, this condition could arise in an optical waveguide which possesses no differential modal attenuation and no mode coupling. The steady state would not represent a unique distribution in this case. Under the same conditions the EMD, as we have used it, is undefined. Most authors do not draw a distinction between steady-state and EMD conditions. Following this precedent, we also will use both terms to apply to any length-independent modal distribution.

coupling. This implies that such fibers, which also possess differential modal attenuation, will not have a well-characterized EMD for reasonably short (km) lengths of fiber [31,32]. Nevertheless, it has been found desirable to specify fiber attenuation with a restricted input mode volume (or limited phase space) launch condition [32,33] which may be considered to be an approximation to the EMD. In this situation, normalized (dB/km) loss values are less dependent on fiber length and also less sensitive to small variations in launch conditions. This enables the fibers to be characterized in a more reproducible manner and with an improved agreement between different measurement laboratories. Moreover, specifications made with these conditions enable system designers to predict more accurately the total loss of a link consisting of several concatenated fibers, since the attenuation of the components will tend to add in a linear fashion.

## 4.2 Standard Fiber Optic Test Procedures

As part of a general effort to promote consistent measurement techniques for characterizing optical fibers, several standards groups have proposed uniform test procedures. International organizations include the International Electrotechnical Commission (IEC), and the International Telegraph and Telephone Consultative Committee (CCITT) [34,35]. In the U.S., the Electronic Industries Association (EIA) has taken a lead in promoting optical fiber standards and specifications as well as test methods. Approximately sixty test-procedure areas are currently under study, and many are available as the EIA Recommended Standard (RS) 455, and amendments.[9] At the time of this writing (August 1982), the preferred measurement procedures for attenuation, launch conditions, and OTDR are in the draft stage and are being circulated for comment. The documents relevant to the present discussion are: Fiber Optic Test Procedure (FOTP) 46 "Spectral Attenuation Measurement for Long-Length, Graded-Index Optical Fibers," FOTP-53 "Light-Launch Conditions for Long-Length Graded-Index Optical Fiber Spectral Attenuation Measurements," FOTP-54 "Mode Scrambler Launch Requirements for Information Transmission Capacity Measurements," and FOTP-59 "Optical Time-Domain Reflectometry."[10] The test procedures for attenuation are intended to promote repeatable, accurate attenuation measurements that minimize the dependence on fiber length. Several recent publications have discussed some of these recommendations in detail [36,37,38]. We will briefly review here the essentials of these documents as they relate to the current experiments.

The FOTP-46 reference attenuation techniques are based on a cutback method. Here the optical power level $P_1$ is measured through a known ($\gtrsim$1 km) length of near-parabolic graded-index test fiber. A short length (about 2 m) is then cut off the input end of the test fiber without disturbing the original launch conditions. The output power $P_2$ of this short length is determined as before. The attenuation per unit length is then given by the relation

$$\alpha = \frac{-10}{L} \log(P_1/P_2) \qquad \text{(dB/km)} \tag{4-2}$$

where L is the length of the fiber (km) after the short length has been removed. The attenuation is normalized to unit length under the assumption of steady-state conditions. Measurements are usually

[9] EIA Standards Publications: Standards Sales Office, Electronic Industries Association, 2001 Eye St., N.W., Washington, DC 20006. A free catalog of EIA standards publications is available on request. Some of these recommended standards are: RS-455 (and amendments 1-4) "Standard Test Procedures for Fiber Optic Fibers, Cables, Transducers, Connecting and Terminating Devices," RS-458 "Standard Optical Waveguide Fiber Types," and RS-459 "Standard Optical Waveguide Fiber Material Classes."
[10] At the present time, this document contains no recommendations as to preferred launching conditions.

made with a tungsten source of radiation which produces a fairly constant amplitude. This light is suitably filtered to provide the desired wavelength interval.[11] The optical beam is mechanically chopped and synchronously detected.

The FOTP-53 insertion loss technique is similar to the cutback method except that the power $P_2$ is measured through a short length of reference fiber similar to the test fiber. This method is preferred in circumstances where the test fiber cannot be cut. We will in future refer to both the cutback and insertion approaches as "two-point" methods.

There are two acceptable methods described in FOTP-50 for launching light into the test fiber; these are referred to as the beam optics and mode filter[12] techniques. Both involve underfilling the fiber. The beam optics approach uses discrete optical components to control the input numerical aperture (NA) and spot size of the beam on the input face of the fiber. At the present time, the EIA recommends a radiation spot diameter equal to 70 ± 5 percent of the test fiber core diameter, and an input NA equal to 70 ± 5 percent of the nominal fiber NA. Numerical apertures are defined in terms of the sine of the half angle where the intensity has decreased to 5 percent of the maximum value.

The second acceptable method for achieving selective mode excitation may be done by initially overfilling the test fiber; that is, the input beam has a uniform intensity over the face of the fiber and the launch NA exceeds the NA of the fiber. The higher-order modes are then stripped off by means of a mode filter.

## 4.3 Special Problems of OTDR Launch Conditions

In addition to the previously discussed problems of modal energy distributions in the forward direction, accurate backscatter measurements of attenuation entail a careful control of the backward propagating energy also. Backscatter methods in optical fibers always give an indication of round-trip loss, and therefore, for proper interpretation the loss should be the same in both propagation directions [2]. From simple Rayleigh scattering considerations, one would expect the angular dependence of backscattered radiation to vary as $(1 + \cos^2\theta)$, where $\theta$ is the angle between the fiber axis and the direction of propagation of scattered radiation at the point where the scattering occurs. This distribution is approximately isotropic and therefore one might naively assume that the fiber is effectively overfilled in the backward direction. That is, all the modes including leaky and high-order lossy modes are equally excited at each scattering interval in the fiber. There is some experimental evidence indicating that this interpretation is not entirely correct [40-43]. Rather, there are modes which are preferentially excited in the backward direction. These modes tend to be the same as those excited in the forward direction, but this excitation is not complete. In any event, there

[11]The EIA recommends 3 db spectral optical bandwidths of 25 nm or less. By way of comparison, a typical single heterostructure diode source used in OTDR applications has a spectral width of about 5 to 10 nm.

[12]There has been some confusion in the literature on use of the terms "mode filter," "mode scrambler," "mode mixer," and "mode stripper." In the interest of clarity, we quote definitions of these quantities given in the Optical Waveguide Communications Glossary [39]:

Mode filter: A device used to select, reject, or attenuate a certain mode or modes.

Mode mixer: Synonym for mode scrambler.

Mode scrambler: A device composed of one or more optical fibers in which strong mode coupling occurs. Frequently used to provide a mode distribution that is independent of source characteristics. In our context, this device is positioned between the light source and the beamsplitter or coupler. Various types of mode scramblers are described in the EIA publication FOTP-54.

Mode stripper: A device that encourages the conversion of cladding modes to radiation modes; as a result, the cladding modes are stripped from the fiber. Some device examples are given in reference 40.

will be, in general, a lack of symmetry in the modal power distributions in the forward and reverse directions of propagation. This effect, coupled with differential modal attenuation, can produce inaccuracies in estimates of fiber attenuation when measurements are made form one end of the fiber only. We conclude then, that it is desirable to control the mode volumes in such a way that symmetry of fiber properties is preserved in both directions of propagation; both launch and recovery conditions must be specified. To accomplish this, it is reasonable to examine the same devices which are used for controlling mode volumes in the two-point reference attenuation set-ups. As adapted for backscatter applications, they are:

1. Beam optics. An example of a possible OTDR system using beam optics to limit the phase space in both launch and recovery is illustrated in figure 3-7. The test spot size $d_t$ and launch NA can be adjusted to satisfy the 70/70 criterion by appropriate control of focal lengths of lenses $L_1$ and $L_2$ and aperture area A. It is a well-known fact that, for graded-index fibers, both spot size and NA must be controlled in order to genrate a given mode volume [44]. In order for the forward traveling and backscattered radiation to be filtered in a similar fashion, the pinhole aperture in figure 3-7 must be added. This aperture is in the focal plane of lens $L_3$ which also coincides with the image of the face of the test fiber. The size of the pinhole in combination with the aperture A at lens $L_2$ can provide the necessary symmetrical mode filtering.

   The beam optics approach has the advantage of giving good control over the radiation being launched and recovered. Disadvantages include complexity and alignment difficulties. Also, this system tends to introduce greater loss (about 6 dB one way) than other methods for restricting the mode volume. Excessive loss is always a concern in OTDR systems.

   Another practical problem involves positioning the input pulse beam accurately on the fiber face. Many OTDR systems do not have provision for visual observation of the location of the radiation spot on the input end of the fiber. Nor can the output power from the far end of the fiber be monitored. This means that the only practical way of aligning the test fiber for measurements is to maximize the t = 0 backscatter signal. This maximum condition may not occur when the beam is centered on the fiber since higher-order modes often have higher scattering coefficients, and consequently generate larger backscatter signals [45]. This problem is more pronounced with smaller spot sizes.
2. Dummy fibers. A long auxiliary fiber can be inserted in front of, and joined to, the test fiber. If this dummy fiber is initially overfilled, the undesirable high-loss modes are attenuated after a few hundred meters, and the output of the device then approaches a source having the required steady-state conditions [46,47]. A functionally different sort of dummy fiber has been proposed by Mickelson and Eriksrud [48]. They showed that a graded-index dummy fiber which supports fewer guided modes than any segment of the test fiber allowed for a particularly simple theoretical interpretation of the backscatter signature from the test fiber. In particular, under these conditions intrinsic loss can be separated in a quantitative and unambiguous way from the fiber's other characteristic parameters. These authors also showed that this device was effective in controlling mode volumes for two-point attenuation comparisons [49]. An appropriate dummy fiber is probably very similar in its effects to the mandrel wrap and other types of mode filters.
3. Mode filters. The types of mode filters that have been used in connection with cutback attenuation measurements are appropriate for OTDR applications as well. Most of these mode filters operate on the principle of selectively removing power in the higher-order modes

through radiation from macrobends of some sort. Examples are serpentine bend or S-shaped channel types [40], and the linear array of pegs [50]. The mandrel wrap structure is another widely used mode filter that was originally developed at the Bell Telephone Laboratories. It has been described by a number of investigators [36,37,51,52,53], and was also used in the experimental work in this report. A typical configuration consists of five turns of fiber loosely wound on a 1 cm mandrel. Other geometries have been tested and found to produce slightly differing effects [51]. Observation of near-field patterns demonstrates that the mode filter does not produce significant mode mixing [40,53]. Presumably, the same sort of filtering operation occurs to backscattered radiation propagating in the reverse direction. Typically, the backscatter response is reduced 2 to 3 dB compared to the overfill case, when the mandrel wrap is installed. For convenience, and to prevent breakage, the fibe coating is usually left intact. This means that the type of jacketing material and thickness may have some bearing on the filtering action. These effects have not been investigated in detail, but are probably small enough to be safely ignored.

The EIA document FOTP-50 contains some recommended procedures for determining the suitability of mode filters for producing a quasi-EMD. These involve comparing the far-field radiation patterns from short (1 to 2 m) and long lengths (1 m) of test fiber. An acceptable mode filter for a particular fiber is defined as one which produces in the short length a far-field maximum radiation angle which is -3 ± 3 degrees less than the comparable radiation angle in the unfiltered long length of fiber.[13] These radiation patterns are matched under conditions that overfill the fiber at the input end. Measurements of this sort on each test fiber are obviously not practical, or even possible, for OTDR measurements. Therefore, a nominal mode filter geometry must suffice. It is suggested that the five-turn/1 cm device may be a satisfactory compromise for this application. It has been shown that, for higher quality fibers, the loss is insensitive to the exact nature of the mode filter [52,54]. Therefore, small performance differences in individual mode filters should not be a serious problem. Experience has also shown that there is little difference in cutback attenuation values between beam optics and mandrel wraps or serpentine bend mode filters [55].

In addition to the aforementioned problems related to reference launch conditions, there is an additional difficulty involved in producing a uniform excitation beam. Most OTDRs use semiconductor single heterojunction laser diodes as sources. These devices emit radiation from a surface having a stripe geometry. A typical structure might have dimensions of 2 by 150 μm. If this source is focused directly on the face of the test fiber, it will not produce a uniform modal excitation. This complication can be avoided by using a mode scrambler between the laser diode source and the beamsplitter (or directional coupler). In the present work we have used a short length (2 m) of step-index fiber, which has been shown to produce a fairly uniform radiation pattern [56].

## 4.4 Experimental Backscatter Results

Recently, NBS conducted an interlaboratory attenuation comparison with nine fiber and cable manufacturers. Attenuation measurements were made on three graded-index multimode fibers with near-parabolic profiles using the recommended EIA cutback techniques. The comparisons give an indication

[13] The width of the radiation patterns is defined in terms of 5 percent (-13 dB) irradiance levels relative to the peak irradiance.

of the practical measurement variance to be expected when standard experimental conditions are used. The fibers were chosen from several manufacturers and represented a diversity of properties. A description of these fibers along with details of the intercomparison are given in reference 55. We felt it would be instructive to subject these same fibers to a backscatter/two-point attenuation comparison on our optical time-domain reflectometer. Many comparisons between the cutback and backscatter-derived attenuation values have been made in the past which indicate that highly accurate and reproducible results are possible [1,57-64]. These previous results, however, usually have been obtained from fibers originating at one laboratory only, and measured under launch conditions which were not made explicit. Part of the objective of the present work was to observe the effect of the mandrel wrap mode filter on the backscatter attenuation values in several well-characterized fibers from different manufacturers.

We have described elsewhere the construction details and performance characteristics of the optical time-domain reflectometer used in the present experiments [4]. A block diagram of the system is shown in figure 4-1, along with some slight modifications required for the current work. Backscatter measurements were made with both overfill conditions and with restricted mode volume conditions using the mandrel wrap mode filter. The signals were averaged on a boxcar integrator and the data was then processed using a microcomputer. Some typical scans for the round robin fibers A, C, and D are shown in figures 4-2 to 4-6. Attenuation values were estimated directly from one-half the loss indicated on the vertical axis in these figures.

The OTDR attenuation values are listed in table 4 for both overfill (OF) and restricted launch (LR) conditions. The restricted mode volume launch was always accomplished through the mandrel wrap for the backscatter measurements; the two-point measurements included both beam-optic and mandrel wrap data. The OTDR values represent the average of four readings, two taken from each end of the fiber.

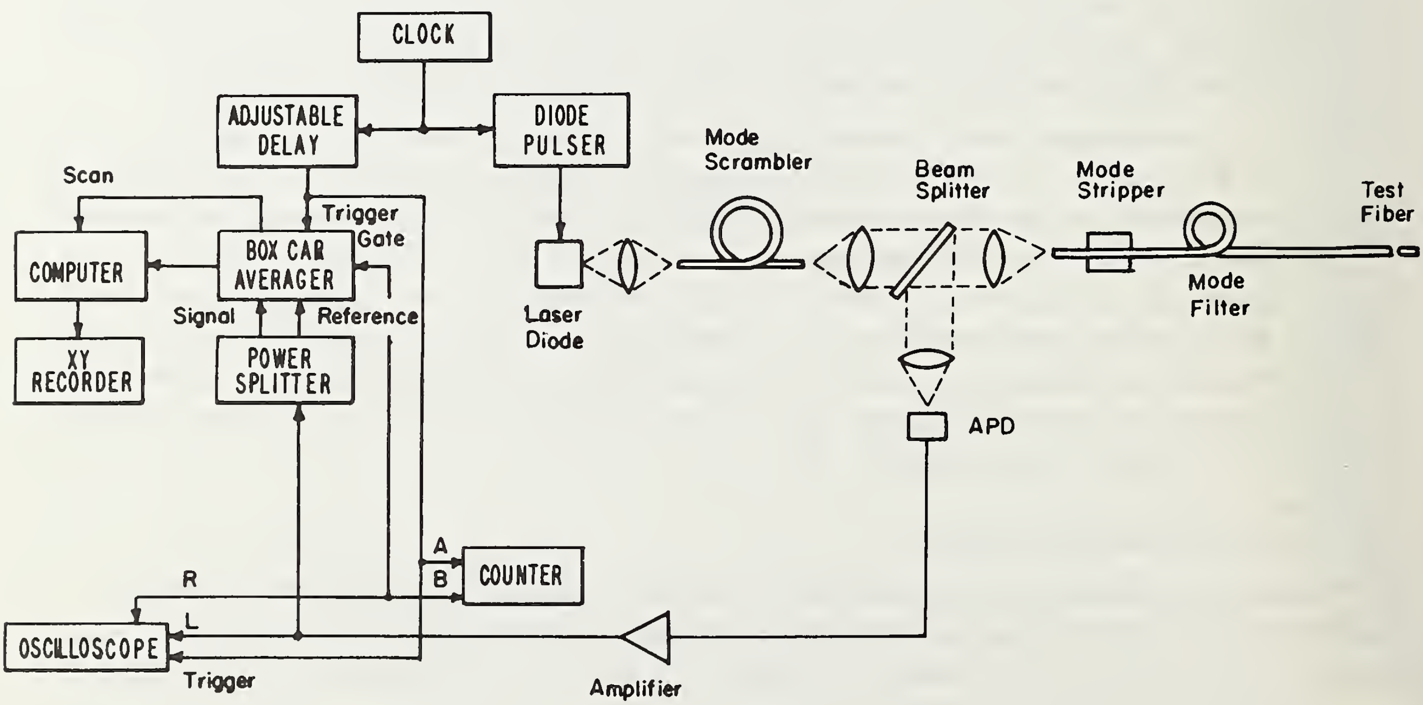


Figure 4-1. Block diagram of the experimental apparatus used for attenuation estimates.

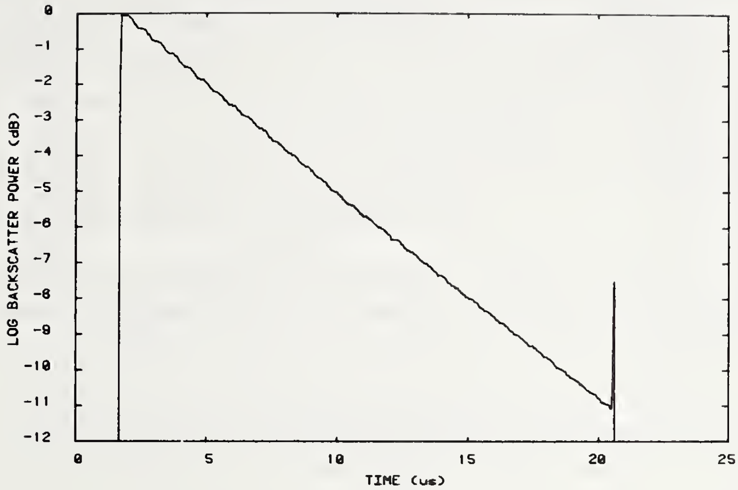


Figure 4-2. Fiber A backscatter signature with overfill excitation conditions.

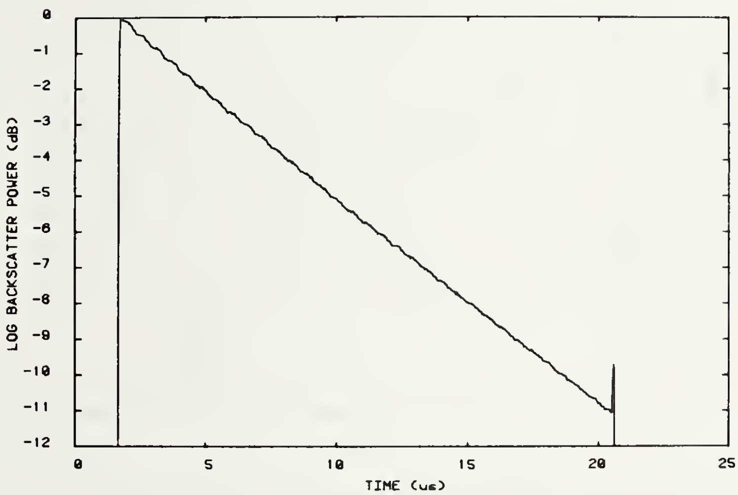


Figure 4-3. Fiber A backscatter signature with mode-filtered excitation conditions.

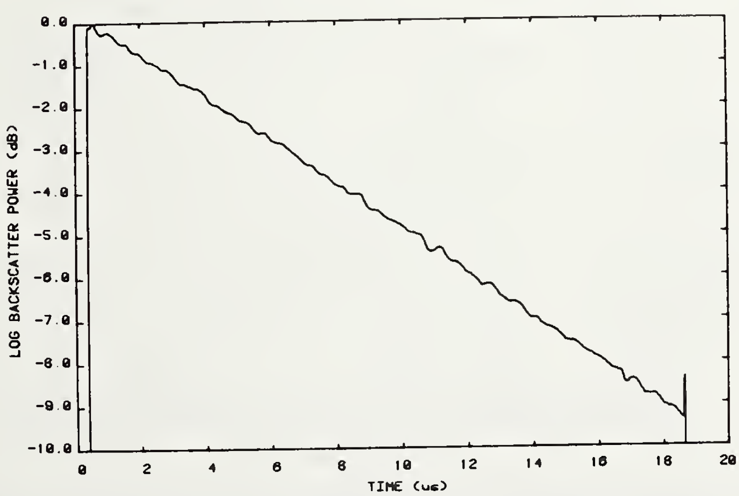


Figure 4-4. Fiber C backscatter signature with overfill excitation conditions.

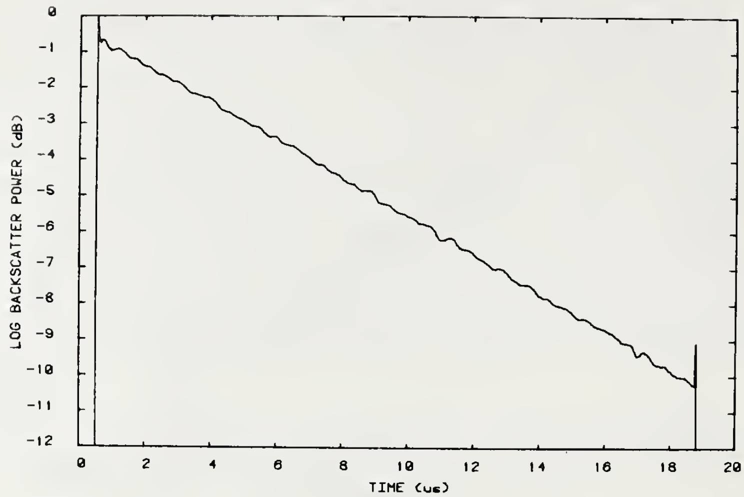


Figure 4-5. Fiber C backscatter signature with mode-filtered excitation conditions.

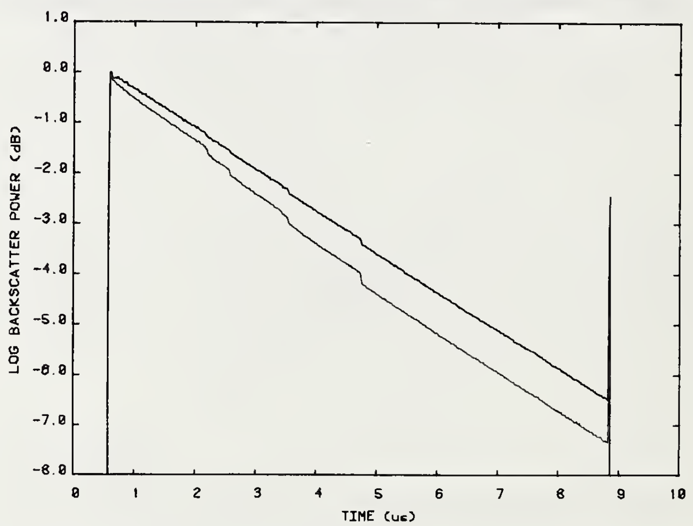


Figure 4-6. Fiber D backscatter signatures; upper trace with overfill excitation conditions, lower trace with mode-filtered excitation conditions.

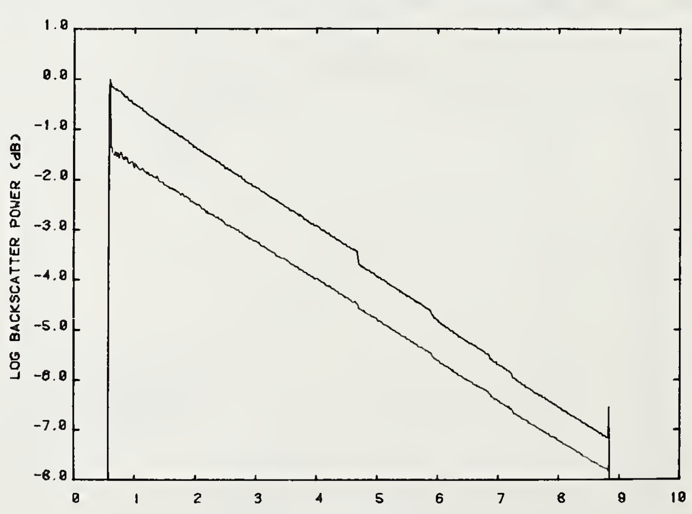


Figure 4-7. Fiber D backscatter signatures excited from opposite end to that in figure 4-6. Upper trace with overfill excitation conditions, lower trace with mode-filtered excitation conditions.

The difference in attenuation values obtained from either fiber end is an indication of the uniformity of fiber properties (particularly numerical aperture) and, hence, a measure of the sort of accuracy obtainable from single-ended measurements. It is clear from the data that, in these examples, the directional properties are small. The stated error limits are one standard deviation values for measurements regardless of which end was used. Also in table 4, the cutback values from reference [54] are listed for comparison. In this case, the error limits are the one sigma values indicating the spread in measurement values among the nine test groups.

We can draw the following conclusions from the data listed in table 4.

1. For both the OTDR and cutback cases, the extreme difference in attenuation values between the overfill and restricted launch conditions amounts to a few tenths of a decible/kilometer. Attenuation values are usually higher for the overfill conditions.
2. The two-point/OTDR agreement is better with the restricted launch conditions. In this case, the one sigma limits overlap for the two types of measurements. This comparison suggests that the two different approaches for determining fiber loss can agree within the experimental precision of current measurement techniques.

The signatures shown in figures 4-2 to 4-7 provide additional information concerning the fiber attenuation as a function of length. In particular, we can observe the effect of the mode filter on the backscatter response. Recalling that the instantaneous slope of the signature on the semilog plot of backscatter power versus time can be identified with the fiber loss at that point,[14] a curvature in the slope indicates a nonequilibrium loss condition. The overfilled fiber D (fig. 4-7), for example, shows a slope curvature in the first microsecond or so, while the counterpart mode-filtered signature shows a uniform slope in this time interval. This implies that transient high-order, high-loss modes have been removed, resulting in a certain local equilibrium mode distribution. This is the way the mode filter is supposed to work. However, this type of response is not obtained from all fibers. Fiber A (figs. 4-2 and 4-3) shows some curvature over the length of the fiber, but this curvature is not affected to any great extent by the presence of the mode filter. Fiber C (figs. 4-4 and 4-5) exhibits a fairly constant slope in the long term (1 to 18 μs) both with and without the mode filter (the fluctuations with frequency around 0.5 μs are due to diameter changes). This also indicates that

Table 4. Comparison of cutback and OTDR attenuation values. Launch condition OF indicates overfill, RL restricted launch. Error limits are one sigma values.

| Fiber | OTDR launch condition | Attenuation OTDR (dB/km) | Attenuation cutback (dB/km) |
|---|---|---|---|
| A | OF | 2.90 ± 0.01 | 3.34 ± 0.39 |
| A | RL | 2.89 ± 0.02 | 2.92 ± 0.24 |
| C | OF | 2.54 ± 0.01 | 2.60 ± 0.04 |
| C | RL | 2.59 ± 0.01 | 2.57 ± 0.12 |
| D | OF | 4.24 ± 0.06 | 4.69 ± 0.47 |
| D | RL | 3.87 ± 0.08 | 3.89 ± 0.43 |

[14]As mentioned previously, there are certain cases where this identification may not be correct, but for slowly changing optical properties of the fiber, it serves as a useful approximation.

there is little differential mode attenuation and that removing the higher-order modes does not affect the loss significantly. These examples, and others not shown here, are consistent with the assumption that backscatter signatures generated with the mandrel wrap mode filter will demonstrate less short-term, nonequilibrium loss features than if the mode filter is not used.

Fiber D was fusion spliced in the center and exhibited an abrupt drop in backscatter power at that point. It will be noted that the apparent splice loss, inferred from the magnitude of this drop, is a strong function of excitation conditions. The apparent loss also depends on which end is used for measurement purposes.

## 5. Conclusions

For the most accurate attenuation measurements, the linearity of the time-domain reflectometer should be carefully checked since the avalanche photodiode detectors used in these devices can easily be driven into a nonlinear response region. Properly designed systems are capable of linear dynamic ranges in excess of 40 dB (optical).

A widely accepted reference test procedure for the measurement of attenuation in long lengths of graded-index fibers, has been promulgated by the Electronics Industries Association. This method involves the two-point power transmission measurement technique. The backscatter method of estimating attenuation, for a number of reasons, will probably not equal this approach in accuracy. However, OTDR estimates are often more convenient to make, and if good agreement with standard methods is a consideration, it is desirable to control experimental conditions in such a way that two-point and backscatter values are consistant and discrepancies in the two techniques are minimized. Some of the uncertainties associated with the backscatter measurements can be reduced by closely simulating the EIA recommended two-point launch conditions. One possible approach is to use overfill launch conditions in conjunction with a mode filter in the OTDR system. These devices filter the radiation in both the forward and backward propagation directions. This implies that undesired higher-order backscattered modes excited by the Rayleigh scattering process are removed from detection. It also means that it is not possible to duplicate exactly the modal power distributions in the two attenuation methods; the mode filtering occurs twice (launch and recovery) in the backscatter case and only once (launch) with the transmission measurements. Nevertheless, the mode filters tend to promote a quasi-steady-state mode distribution in most fibers which is necessary for precise attenuation estimates. An appropriate dummy fiber can be used for this purpose. We have investigated the mandrel wrap mode filter in the present work and found that it produces a reasonably uniform modal power distribution as determined from backscatter signatures. The experimental results indicate that, while the mandrel wrap mode filter produces slightly different effects on different types of fiber, it is effective in removing any undesired excessively lossy transient modes. This type of restricted launch does not require special equipment, has the virtue of convenience and can be adapted to field use. We have also shown that excellent agreement is possible in comparisons between the cutback and backscatter-derived attenuation values, when the mandrel wrap filter is used in measurements on stable, well-characterized test fibers.

## 6. References

[1] Barnoski, M. K.; Jonson, S. M. Fiber waveguides: A novel technique for investigating attenuation characteristics. Appl. Opt. 15(4):2112-2115; 1976 September.

[2] Danielson, B. L. An assessment of the backscatter technique as a means for estimating loss in optical waveguides. Nat. Bur. Stand. (U.S.) Tech. Note 1018; 1980 February. 76 p.

[3] Danielson, B. L. Backscatter measurements on optical fibers. Nat. Bur. Stand. (U.S.) Tech. Note 1034; 1981. 44 p.
[4] Danielson, B. L. Backscatter signature simulations. Nat. Bur. Stand. (U.S.) Tech. Note 1050; 1981. 100 p.
[5] Schinke, D. P.; Smith, R. G.; Hartman, A. R. Photodetectors, chapter 3 in Semiconductor devices for optical communication: Topics in applied physics, Vol. 39. H. Kressel, ed. New York: Springer-Verlag; 1980. 63-85.
[6] Sharma, A. B.; Halme, S. J.; Butusov, M. M., eds. Optical fiber systems and their components. New York: Springer-Verlag; 1981. 242 p.
[7] Webb, P. P.; McIntyre, R. J.; Conradi, J. Properties of avalanche photodiodes. RCA Rev. 35:234-278; 1974 June.
[8] Misugi, T.; Takanashi, H. Detectors for optical fiber communications. Tech. Digest, 1977 Int. Conf. on Integrated Optics and Optical Fiber Communication; 1977 July 18-20; Tokyo, Japan; 33-36.
[9] Smith, R. G. Photodetectors for fiber transmission systems. Proc. IEEE 68(10):1247-1253; 1980 October.
[10] Pearsall, T. P. Photodetectors for optical communication. J. Opt. Commun. 2(2):42-48; 1981 June.
[11] Melchior, H.; Fisher, M. B.; Arams, F. R. Photodetectors for optical communication systems. Proc. IEEE 1466-1486; 1970 October.
[12] Carni, P. Photodetectors, chapter 2 in Optical fiber communication. New York: McGraw-Hill; 1980. 471-496.
[13] Personick, S. D. Photodetectors for fiber systems, chapter 5 in Fundamentals of optical fiber communications. M. K. Barnoski, ed. New York, NY: Academic Press; 1981. 257-293.
[14] Stillman, G. E.; Wolfe, C. M. Avalanche photodiodes, chapter 5, in Semiconductors and semimetals, Vol. 12. R. K. Willardson and A. C. Beer, eds. New York, NY: Academic Press; 1977. 291-381.
[15] Muller, J. Photodiodes for optical communication, in Advances in electronics and electron physics, Vol. 55. L. Marton and C. Marton, eds. New York, NY: Academic Press; 1981. 189-308.
[16] Murray, L. A.: Wana, K.; Hesse, K. A review of avalanche photodiodes, trends and markets. Opt. Spectra :54-59; 1980 April.
[17] Lee, T. P.; Li, T. Photodetectors, chapter 18 in Optical fiber telecommunications. S. E. Miller and A. G. Chynoweth, eds. New York, NY: Academic Press; 1979. 593-626.
[18] Keyes, R. J. Optical and infrared detectors, vol. 19 in Topics in applied physics. New York, NY: Springer-Verlag; 1980.
[19] Melchior, H. Demodulation and photodetection techniques, chapter C7 in Laser handbook, Vol. 1. F. T. Arecchi and E. O. Schulz-Dubois, eds. New York, NY: American Elsevier Publishing Co.; 1972. 725-835.
[20] Anderson, L. K.; Di Domenico, M., Jr.; Fisher, M. B. High speed photodetectors for microwave demodulation of light, in Advances in microwaves, Vol. 5. L. Young, ed. New York, NY: Academic Press; 1970. 1-121.
[21] See, for example, table 10 in reference 15.
[22] Carr, D. L.; Shaunfield, W. N., Jr. Back-to-basics with avalanche photodiodes. Electro-Optical Syst. Design, 46-50; 1979 July.
[23] Melchior, H.; Hartman, A. R.; Schinke, D. P.; Seidel, T. E. Planar epitaxial silicon avalanche photodiode. Bell Syst. Tech. J. 57(6):1791-1807; 1978 July-August.
[24] Carni, P. G. Photodetectors, chapter 2 in Optical fiber communication, Technical staff of CSELT. New York, NY: McGraw-Hill Book Co. 1981. 471-497.
[25] Some commercial products are identified in this report in order to specify precisely experimental conditions. This does not constitute an endorsement; other products may serve equally well.
[26] Reference 19, page 793.
[27] Neumann, E. G. Analysis of the backscattering method for testing optical fiber cables. AEÜ, Electron. Commun. 34(4):157-160; 1980.
[28] DiVita, P.; Rossi, V. Backscattering measurements in optical fibers: separation of power decay from imperfection contribution. Electron. Lett. 15(5):467-469; 1979 July 19.
[29] Cherin, A. H.; Cohen, L. G.; Holden, W. S.; Burrus, C. A.; Kaiser, P. Transmission characteristics of three Corning multimode optical fibers. Appl. Opt. 13(10):2359-2364; 1974 October.
[30] Olshansky, R.; Oaks, S. M. Differential mode attenuation measurements in graded-index fibers. Appl. Opt. 17(11):1830-1835; 1978 June 1.
[31] Holmes, G. T.; Hawk, R. M. Limited phase-space attenuation measurements of low-loss optical waveguides. Opt. Lett. 6(2):55-57; 1981 February.
[32] Hawk, R. M. Multimode waveguide attenuation measurements. Tech. Digest, Symposium on Optical Fiber Measurements; 1980 October 28-29; Boulder, CO. Nat. Bur. Stand. (U.S.) Spec. Publ. 597; 1980 October. 1-9.
[33] Reitz, P. Measuring optical waveguide attenuation: The LPS method. Opt. Spectra 15(8):48-52; 1981 August.

[34] Love, R. E. Waveguide fiber standards. Tech. Digest, Symposium on Optical Fiber Measurements; 1980 October 28-29; Boulder, CO. Nat. Bur. Stand. (U.S.) Spec. Publ. 597; 1980 October. 135-143.
[35] Standards for fiberoptics; Laser Focus 17(5):110-118; 1981 May.
[36] Chipman, J. D. Measurement standards for optical fiber in field installations. Laser Focus 18(7):99-106; 1982 July.
[37] Cherin, A. H.; Gardner, W. B. Fiber measurement standards. Laser Focus 16(8):60-65; 1980 August.
[38] Franzen, D. L.; Day, G. W.; Gallawa, R. L. Standardizing test conditions for characterizing fibers. Laser Focus. 17(8):103-105; 1981 August.
[39] Hanson, A. G.; Bloom, L. R.; Cherin, A. H.; Day, G. W.; Gallawa, R. L.; Gray, E. M.; Kao, C.; Kapron, F. P.; Kawasaki, B. S.; Reitz, P.; Young, M. Optical waveguide communications glossary. Nat. Bur. Stand. (U.S.) Handb. 140; 1982 January. 33 p.
[40] Stone, F. T.; Krawarik, P. H. Mode elimination in fiber loss measurements. Appl. Opt. 18(6):756-758; 1979 March 15.
[41] Payne, R. Modal distribution of backscattered light in a step-index multimode fibre. Electron. Lett. 17(16):568-570; 1981 August 6.
[42] Costa, B.; DiVita, P.; Morra, P.; Rossi, V.; Sordo, B. Backscattered mode power distribution in optical fibres. Post-Deadline Papers, 7th European Conference on Optical Communication; Copenhagen, Denmark; 1981 September 8-11. 29-31.
[43] Costa, B.; Morra, P.; Sordo, B. Power distribution of backward scattered radiation in optical fibers. Tech. Digest, 3rd International Conference on Integrated Optics and Optical Fiber Communication; 1981 April 27-29. San Francisco, CA. p. 76.
[44] Costa, B.; Sordo, B. Fiber characterization, chapter 3 in Optical fiber communication, technical staff of CSELT. New York, NY: McGraw-Hill 1981. 145-296.
[45] Jensen, S. M. Observation of differential mode attenuation in graded-index fiber waveguides using OTDR. Tech. Digest, Topical Meeting on Optical Fiber Communication, 1979 March 6-8; Washington, DC. 120-122.
[46] Tateda, M.; Horiguchi, T.; Tokuda, M.; Uchida, N. Optical loss measurement in graded-index fiber using a dummy fiber. Appl. Opt. 18(19):3272-3275; 1979 October 1.
[47] Holmes, G. T. Launch dependent attenuation measurements on a 10-kilometer concatenation experiment. Tech. Digest, 6th European Conference on Optical Communication. 1980. 16-19 September; York, U.K. 144-147.
[48] Mickelson, A. R.; Eriksrud, M. Theory of the backscattering process in multimode optical fibers. Appl. Opt. 21(11):1898-1909; 1982 June 1.
[49] Eriksrud, M.; Mickelson, A. R.; Lauritzen, S.; Ryen, N. Influence of differential mode attenuation on backscattering attenuation measurements. Tech. Digest, Symposium on Optical Fiber Measurements; 1982 October 13-14; Boulder, CO. Nat. Bur. Stand. (U.S.) Spec. Publ. 641.
[50] Tokuda, M.; Sikai, S.; Yochida, K.; Uchida, N. Measurement of baseband frequency response of multimode fiber by using a new type of mode scrambler. Electron. Lett. 13(5):146-147; 1977.
[51] Cherin, A. H.; Head, E. D. A fiber concatenation experiment using a standardized loss measurement method. Tech. Digest, Symposium on Optical Fiber Measurements; 1980 October 28-29; Boulder, CO. Nat. Bur. Stand. (U.S.) Spec. Publ. 597; 1980 October. 19-22.
[52] Kaiser, P. Loss measurements of graded-index fibers: accuracy versus convenience. Tech. Digest, Symposium on Optical Fiber Measurements; 1980 October 28-29; Boulder, CO. Nat. Bur. Stand. (U.S.) Spec. Publ. 597; 1980 October. 11-14.
[53] Miller, C. M.; Kummer, R. B. Direct measurement of mode coupling effects using a mandrel wrap mode filter. Tech. Digest, 6th European Conference on Optical Communication. 1980 September 16-19; York, England. 99-102.
[54] Eriksrud, M.; Hordvik, A.; Ryen, N.; Nakken, G. Comparison between measured and predicted transmission characteristics of 12 km spliced grade-index fibers. Opt. Quantum. Electron. 11(6):517-523; 1979 November.
[55] Franzen, D. L.; Day, G. W.; Danielson, B. L.; Chamberlain, G. E.; Kim, E. M. Interlaboratory measurement comparison to determine the attenuation and bandwidth of graded-index optical fibers. Appl. Opt. 20(14):2412-2419; 1981 July 15.
[56] Tanifuji, T.; Horiguchi, T.; Tokudi, M. Baseband-frequency response measurement of graded-index fiber using step-index fiber as an exciter. Electron. Lett. 15(7):203-204; 1979 March 29.
[57] Costa, B.; Sordo, B. Experimental study of optical fiber attenuation by modified backscattering technique. Tech. Digest, 3rd European Conference on Optical Communication; 1977 September 14-16; Munich, Germany. 69-71.
[58] Barnoski, M. K.; Rourke, M. D.; Jensen, S. M.; Melville, R. T. Optical time domain reflectometer. Appl. Opt. 16(9): 2375-2379; 1977 September.
[59] Rourke, M. D. An overview of optical time-domain reflectometry, in Physics of Fiber Optics, Vol. 2. Advances in Ceramics, B. Bendrow and S. S. Mitra, eds. Columbus, OH: American Ceramic Society, Inc.; 1980. 252-272.
[60] Costa, B.; Sordo, B.; Menaglia, U.; Piccari, L.; Grasso, G. Attenuation measurements performed by backscattering technique. Electron. Lett. 16(10):352-353; 1980 May 8.
[61] Conduit, A. J.; Hartog, A. H.; Payne, D. N. Spectral- and length-dependent losses in optical fibers investigated by a two-channel backscatter technique. Electron. Lett. 16(3):77-78; 1980.

[62] Costa, B.; DeBernardi, C.; Sordo, B. Investigation of scattering characteristics and accuracy of the backscattering technique by wavelength dependent measurements. Tech. Digest, 4th European Conference on Optical Communication; 1978 September 12-15; Genoa, Italy. 140-145.

[63] Eriksrud, M.; Lauritzen, S.; Ryen, N. Backscatter attenuation measurements in graded-index fibers. Electron. Lett. 16(23):877-879; 1980 November 6.

[64] Costa, B. Comparison between various fiber characterization techniques. Tech. Digest, 5th European Conference on Optical Communication, post-deadline supplement; 1979 September 17-19; Amsterdam, Netherlands. II-1, II-5.

NBS-114A (REV. 2-80)

| U.S. DEPT. OF COMM. BIBLIOGRAPHIC DATA SHEET *(See instructions)* | 1. PUBLICATION OR REPORT NO. NBS TN-1065 | 2. Performing Organ. Report No. | 3. Publication Date June 1983 |
|---|---|---|---|

**4. TITLE AND SUBTITLE**

Optical Time-Domain Reflectometer Performance and Calibration Studies

**5. AUTHOR(S)**

B. L. Danielson

**6. PERFORMING ORGANIZATION** *(If joint or other than NBS, see instructions)*

NATIONAL BUREAU OF STANDARDS
DEPARTMENT OF COMMERCE
WASHINGTON, D.C. 20234

**7. Contract/Grant No.**

**8. Type of Report & Period Covered**

**9. SPONSORING ORGANIZATION NAME AND COMPLETE ADDRESS** *(Street, City, State, ZIP)*

Communications Systems Center
U.S. Army Communications R&D Command
Fort Monmouth, New Jersey 07703

**10. SUPPLEMENTARY NOTES**

☐ Document describes a computer program; SF-185, FIPS Software Summary, is attached.

**11. ABSTRACT** *(A 200-word or less factual summary of most significant information. If document includes a significant bibliography or literature survey, mention it here)*

The measurement accuracy of the optical time-domain reflectometer (OTDR) is restricted in some applications by a limited operational dynamic range and by a lack of standardized test procedures. In an effort to better understand these restrictions, we have measured the range of linearity of some avalanche photodiodes used as backscatter detectors. Also, the effect of input launch conditions is examined and a possible standardized OTDR test procedure is proposed. Using these suggestions, we have made comparisons between attenuation values determined by cutback and backscatter methods and found that good agreement is possible. Finally, some methods are described for checking the response linearity of OTDR systems.

**12. KEY WORDS** *(Six to twelve entries; alphabetical order; capitalize only proper names; and separate key words by semicolons)*

APD; avalanche photodiodes; backscattering; backscatter signatures; optical fiber scattering; optical time-domain reflectometer; OTDR

**13. AVAILABILITY**

☒ Unlimited
☐ For Official Distribution. Do Not Release to NTIS
☒ Order From Superintendent of Documents, U.S. Government Printing Office, Washington, D.C. 20402.
☐ Order From National Technical Information Service (NTIS), Springfield, VA. 22161

**14. NO. OF PRINTED PAGES**

32

**15. Price**

$8.50

# NBS TECHNICAL PUBLICATIONS

## PERIODICALS

**JOURNAL OF RESEARCH**—The Journal of Research of the National Bureau of Standards reports NBS research and development in those disciplines of the physical and engineering sciences in which the Bureau is active. These include physics, chemistry, engineering, mathematics, and computer sciences. Papers cover a broad range of subjects, with major emphasis on measurement methodology and the basic technology underlying standardization. Also included from time to time are survey articles on topics closely related to the Bureau's technical and scientific programs. As a special service to subscribers each issue contains complete citations to all recent Bureau publications in both NBS and non-NBS media. Issued six times a year. Annual subscription: domestic $18; foreign $22.50. Single copy, $4.25 domestic; $5.35 foreign.

## NONPERIODICALS

**Monographs**—Major contributions to the technical literature on various subjects related to the Bureau's scientific and technical activities.

**Handbooks**—Recommended codes of engineering and industrial practice (including safety codes) developed in cooperation with interested industries, professional organizations, and regulatory bodies.

**Special Publications**—Include proceedings of conferences sponsored by NBS, NBS annual reports, and other special publications appropriate to this grouping such as wall charts, pocket cards, and bibliographies.

**Applied Mathematics Series**—Mathematical tables, manuals, and studies of special interest to physicists, engineers, chemists, biologists, mathematicians, computer programmers, and others engaged in scientific and technical work.

**National Standard Reference Data Series**—Provides quantitative data on the physical and chemical properties of materials, compiled from the world's literature and critically evaluated. Developed under a worldwide program coordinated by NBS under the authority of the National Standard Data Act (Public Law 90-396).

NOTE: The principal publication outlet for the foregoing data is the Journal of Physical and Chemical Reference Data (JPCRD) published quarterly for NBS by the American Chemical Society (ACS) and the American Institute of Physics (AIP). Subscriptions, reprints, and supplements available from ACS, 1155 Sixteenth St., NW, Washington, DC 20056.

**Building Science Series**—Disseminates technical information developed at the Bureau on building materials, components, systems, and whole structures. The series presents research results, test methods, and performance criteria related to the structural and environmental functions and the durability and safety characteristics of building elements and systems.

**Technical Notes**—Studies or reports which are complete in themselves but restrictive in their treatment of a subject. Analogous to monographs but not so comprehensive in scope or definitive in treatment of the subject area. Often serve as a vehicle for final reports of work performed at NBS under the sponsorship of other government agencies.

**Voluntary Product Standards**—Developed under procedures published by the Department of Commerce in Part 10, Title 15, of the Code of Federal Regulations. The standards establish nationally recognized requirements for products, and provide all concerned interests with a basis for common understanding of the characteristics of the products. NBS administers this program as a supplement to the activities of the private sector standardizing organizations.

**Consumer Information Series**—Practical information, based on NBS research and experience, covering areas of interest to the consumer. Easily understandable language and illustrations provide useful background knowledge for shopping in today's technological marketplace.

*Order the* **above** *NBS publications from: Superintendent of Documents, Government Printing Office, Washington, DC 20402.*

*Order the* **following** *NBS publications—FIPS and NBSIR's—from the National Technical Information Services, Springfield, VA 22161.*

**Federal Information Processing Standards Publications (FIPS PUB)**—Publications in this series collectively constitute the Federal Information Processing Standards Register. The Register serves as the official source of information in the Federal Government regarding standards issued by NBS pursuant to the Federal Property and Administrative Services Act of 1949 as amended, Public Law 89-306 (79 Stat. 1127), and as implemented by Executive Order 11717 (38 FR 12315, dated May 11, 1973) and Part 6 of Title 15 CFR (Code of Federal Regulations).

**NBS Interagency Reports (NBSIR)**—A special series of interim or final reports on work performed by NBS for outside sponsors (both government and non-government). In general, initial distribution is handled by the sponsor; public distribution is by the National Technical Information Services, Springfield, VA 22161, in paper copy or microfiche form.

U.S. Department of Commerce
National Bureau of Standards

Washington, D.C. 20234
Official Business
Penalty for Private Use $300

U.S.MAIL

POSTAGE AND FEES PAID
U.S. DEPARTMENT OF COMMERCE
COM-215

FIRST CLASS